The Cosmological Gene Project: cluster analysis of the atmospheric fluctuations on arcmin-scale imaging of the Cosmic Microwave background

H.E.Jørgensen
Astronomical Observatory, Juliane Maries Vej 30, DK-2100 Copenhagen, Denmark
E.V.Kotok
Theoretical Astrophysics Center, Juliane Maries Vej 30, DK-2100 Copenhagen, Ø Denmark
I.P. Naselsky, P.D.Naselsky, [1]
Rostov State University, Zorge 5, 344090 Rostov-Don, Russia
I.D.Novikov [2]
Theoretical Astrophysics Center, Juliane Maries Vej 30, DK-2100 Copenhagen, Denmark
Yu.Parijskij, P.Tcibulev
Special Astrophys. Obser., Nizhnij Arkhyz, Karachaj-Cherkess Republic, 357147 Russia.
E.V.Vasil'ev
Rostov State University, Zorge 5, 344090 Rostov-Don, Russia

Abstract

We discuss some aspects of the Cosmological Gene Project started at the Special Astrophysical Observatory (Russia) in 1999. The goal of the project is to measure the anisotropy and polarization of the Cosmic Microwave Background (CMB) and investigation of atmospheric fluctuations and foreground on arcmin-scales using the radio-telescope RATAN-600. We develop the cluster analysis of one-dimensional random fields for the application to the RATAN-600 scans. We analyze the specific properties of peak clusterisation in the RATAN-600 scans which to separate the primordial CMB signal from noise.

1 Introduction

The Cosmological Gene Project started at the Special Astrophysical Observatory (SAO RAN, Russia) in 1999 and is devoted to the measurements of anisotropy and polarization of the Cosmic Microwave Background (CMB) with the highest possible angular

[1] Also: Theoretical Astrophysics Center, Juliane Maries Vej 30, DK-2100 Copenhagen; NORDITA, Blegdamsvej 17, DK-2100 Copenhagen, Denmark.

[2] Also: Astro-Space Center of Lebedev Physical Institute, Profsoyuznaya 84/32, Moscow, Russia; Astronomical Observatory, Juliane Maries Vej 30, DK-2100 Copenhagen, Denmark; NORDITA, Blegdamsvej 17, DK-2100 Copenhagen, Denmark.

and multipole resolution (up to $l \leq 10^5$)[3]. This project is carried out by the radio telescope RATAN-600. This is a reflector type instrument, world largest in size and specially designed for high sensitivity and high angular resolution multi-wavelengths measurements in the frequency interval $\nu = 1 - 30$GHz being the optimum for ground based telescopes. For all ground based CMB anisotropy and polarization projects it is important to know the level of the atmospheric emission from water molecules since water vapor in the troposphere close to the condensation point [1,2] is the strongest source of brightness temperature variation.

Investigation of the atmospheric emission (AE) at frequency $\nu = 1 - 30$GHz has been done on RATAN-600 during more than 20 years. The detection level of AE has approached an antenna temperature of a few mK while the CMB signal could be close to a few μK. Thus, in order to reach the level of primordial CMB signal the efficiency of AE filtration has to be extremely high $\succeq 10^3$. It can be obtained by accumulation of observational data at different frequencies and by long term averaging.

Besides that, due to the very large diameter of the antenna ($D \simeq 600$m) the atmospheric noise lies in a so called "near-field zone" of the instrument and are smoothed by the aperture averaging effect. In addition the dual-beam and multi-frequency filtration of the AE signal are especially important for cleaning of the observational records.

The critical point of the AE filtration problem is the estimation of the damping factor of the AE variance. The two following points play an important role for resolving this problem. Firstly, after the CMB experiments already carried out (see for review [3]) we can predict the general character of the CMB anisotropy power spectrum $C(l)$ at the high multipole range $l \gg 10^2$. For the most interesting cosmological model (SCDM, ΛCDM, OpenCDM, etc.) the important property of the spectrum is the exponential decrease at $l \succeq l_d$ where $l_d \approx 10^3$ corresponds the manifestation of the diffusion damping during recombination. This means that at small angular scale $\theta \leq 1$ arcmin ($l \gg l_d$) the observational signal only contains the AE noise and foreground noise (mainly unresolved point sources PS).

Following [4] we can expect that the power spectra at $l \gg l_d$ are: $C_{PS}(l) \propto const$ and $C_{AE} \propto l^{-3}$ for unresolved point sources and atmospheric emission respectively. This means that the extra resolution of the RATAN-600 antenna beam (up to $l \sim 10^4 - 10^5$) allows us to determine the structure of the noise signal at the extremely small angular scale. The next point is connected with the cluster analysis and peak statistics of the CMB+AE+foreground signal in the RATAN-600 scans. We would like to point out that in every 24^h record of the radio sky we can "see" $\sim l_d \simeq 10^3$ maxima and minima connected with the CMB signal and $\sim 10^4 - 10^5$ peaks corresponding to all types of noises (radiometer, AE, PS and so on). In another words, in every RATAN-600 scan we have a wide represented peak statistics due to the CMB signal and the different types of noise as well.

[3]General information about CG-project is available on the web-site www.sao.ru

The second point is related to the statistical properties of the observational signal. One of the most important prediction of the inflation paradigm is the Gaussian character of the CMB anisotropy distribution on the sky. For the AE noise and foreground noise Gaussian fluctuations could be "a lucky chance" only. Thus, in the general case being the combination of the primordial CMB signal and different types of noise in RATAN-600, scans can be non-Gaussian due to the statistical properties of the noise.

P. Naselsky and D. Novikov [5] and D. Novikov and H. Jørgensen [6] pointed out that in this case a cluster analysis of the signal is very effective to separate noise from the signal. The goal of this work is to analyze how the cluster analysis technique can be applied to separate the primordial CMB signal from noise (AE and PS) for the particular case of observations with RATAN-600.

2 Cluster analysis of the one-dimensional random fields

As we mentioned above, the two-dimensional random CMB+AE+foreground signal on the sky is transformed by the RATAN-600 antenna-beam into series of the one-dimensional realization with very high angular resolution. In Fig.1a we plot the result of the weighted average of the 57 records of the AE noise which was obtained at wavelength $\lambda = 1.38$cm at declination $\delta = 41^o$ and angular length of scan $L = 11.3^o$ during the 1998 observational period.

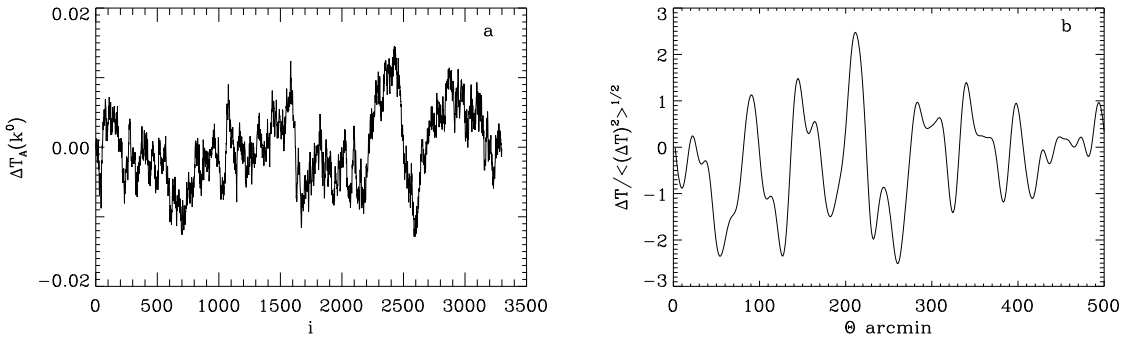

Figure 1: *(a) Scan of weighted average of the 57 records of AE signals. On the x-axis i indicates the step number on the scan with the length $L = 11.3^o$ and with the step size $\Delta x = 12 arcsec$. (b) One-dimensional realization of the primordial CMB signal.*

Fig. 1b shows one theoretical realization realization of the primordial CMB signal, normalized to the variance, which we simulated for the standard cold dark matter

model (SCDM). As one can see from Fig1a,b both signals, CMB and AE, appear approximately uniform and have a lot of maxima and minima. Let us normalize pure CMB fluctuations and AE noise to their variance: $\nu = \Delta T/\sqrt{\langle \Delta T^2 \rangle}$ and consider maxima and minima above some threshold ν_t. Following [5,6] we introduce the definition of a one-dimensional cluster of maxima as the continuous part of the curve with $\nu(t) > \nu_t$ inside the interval $t \in (t_1, t_2)$ where t_1 is one of the roots of the equation $\nu(t_{1,2}) = \nu_t$ and t_2 is the closest root to t_1, $t_2 > t_1$. The length k of the cluster is defined as the number of peaks with height $\nu_{peak} > \nu_t$ in the cluster. If the value of ν_t is high ($\nu_t \gg 1$) then only high maxima of the random field are present above the threshold and the typical length of a cluster is $k = 1$. The reduction of the threshold level ν_t down to $\nu_t \to 0$ or $\nu_t < 0$ leads to the appearance of big clusters when maxima of smaller clusters begin to connect together and generate a new cluster. The investigation of the cluster statistics could have a great potential for probing the nature of CMB and AE signals on the scans. For this purpose, following [5,6],we introduce the number of clusters $N_k(\nu_t)$ of the length k and the total number of clusters $N(\nu_t)$ which are presented in the anisotropy scans for an appropriate threshold ν_t.

$$N(\nu_t) = \Sigma_{k=1}^{\infty} N_k(\nu_t) \tag{1}$$

and the mean length of a cluster at cross level ν_t:

$$\langle k(\nu_t) \rangle = \frac{\Sigma_{k=1}^{\infty} k N_k(\nu_t)}{\Sigma_{k=1}^{\infty} N_k(\nu_t)}. \tag{2}$$

Note that the definitions Eq.(1) and Eq.(2) do not depend on the nature of the initial random signal or its composition.

Let us turn back to the data of AE (see Fig.1a) and take into account that the step on the x-axis is only $\Delta x = 12$arcsec. Such a high angular resolution is wittingly in excess for the analysis of the real data and allows us to use an additional procedure of filtration of noise by smoothing the data. Let us consider the following smoothed array of data Ψ_i:

$$\Psi_i = \frac{\Sigma_j f_i K_{ij}(d)}{\Sigma_j K_{ij}(d)}, \tag{3}$$

where f_i is the initial array of data of Fig.1a, $K_{ij}(d)$ is the filter (see below) with the characteristic scale of smoothing d.

We use below (as one of the possible choices) a Gaussian filter $K_{ij}(d) = \exp(\frac{(i-j)^2}{2d^2})$ for different values of parameter d: $d = 5$, $d = 10$ and $d = 100$. After such a filtration we can easily simulate the rate of clusterisation for the initial and smoothed data. The result of this simulation is represented on Fig.2. As one can see from this figure, while the scale of smoothing d increases from $d = 5$ (which corresponds to the characteristic scale $\alpha \simeq 1$ arcmin) up to $d = 100$ ($\alpha \simeq 20$ arcmin) the mean length of the clusters

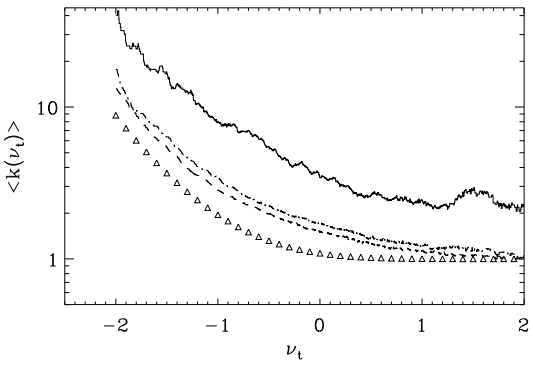

Figure 2: *The mean length of a cluster. From top to bottom: initial AE signal from Fig.1a, smoothed AE signals ($d = 5$ and $d = 10$ correspondingly), pure CMB signal represented by triangles for the SCDM.*

decreases monotonically for a fixed level of the threshold. One can compare this result with the rate of clusterisation (mean length of clusters) of the pure CMB signal (see Fig.2) which is found systematically less than the non smoothed AE data. This tendency become even more pronounced if we use the procedure of filtration of the pure CMB signal with $d = 5 - 10$.

Thus, as one can see from the above result, if we have the same scale of smoothing for the AE signal and the pure CMB signal then the rate of clusterisation of AE noise is always larger than the rate of clusterisation of the pure CMB signal.

In the following we will discuss the theoretical rigor of this phenomenon more precisely. The critical point of our analysis is the hypothesis that the primordial CMB anisotropy distribution on the sky is Gaussian. Observations by RATAN-600 give one-dimensional scans of ΔT. Let us consider a theoretical realization of a one-dimensional slice with Ł $\ll 2\pi$ of the two-dimensional ΔT-field with power spectrum $C_T(l_{ij})$. $\Delta T(x)$ for this one-dimensional slice can be written as follows [5,6]:

$$\Delta T(x) = \sum_{i,j} a_{ij} \sqrt{C_T(l_{ij})} \cos\left(\frac{2\pi}{L} ix + \varphi_{ij}\right) W_{ij}, \tag{4}$$

where a_{ij} are independent Gaussian numbers, $C_T(l_{ij})$ is the power spectrum of fluctuations, φ_{ij} are random phases homogeneously distributed in the interval $(0, 2\pi)$, $l_{ij} = \frac{2\pi}{L}\sqrt{i^2 + j^2}$, W_{ij} is the RATAN-600 antenna-beam. For the uniform Gaussian random process Eq.(4) the two point correlation function has the standard form:

$$C_{obs}(\tau) = \langle \Delta T(x) \Delta T(x') \rangle = \frac{1}{2} \sum_{i,j} a_{ij}^2 J_0(l_{ij}\tau) C(l_{ij}) W_{ij}^2, \tag{5}$$

where $\tau = |x - x'|$. After averaging over the ensemble the correlation function and its variance are [6]:

$$C(\tau) = \frac{\pi}{2} \int dl\ C(l) J_o(l\tau) W^2(l) \tag{6}$$

$$D(\tau) = \overline{C^2_{obs}(\tau)} - [\overline{C_{obs}(\tau)}]^2 = \frac{\pi}{2} \int dl\ C^2(l) J^2_o(l\tau) W^4(l).$$

For investigation of the peak statistics we can introduce the spectral parameters [7]:

$$\sigma^2_p = p! 2^{2p} (-1)^p \frac{d^p C(\tau)}{d(\omega^2)} \mid_{\tau=0}\ , \tag{7}$$

where $\omega = 2 \sin \frac{\tau}{2}$. As it is well known, the following parameters and its combination are the most important for peak statistics:

$$\begin{array}{l} \sigma^2_0 = \pi \int dl l C(l) W^2(l); \quad \sigma^2_1 = \pi \int dl l^3 C(l) W^2(l); \quad \sigma^2_2 = \pi \int dl l^5 C(l) W^2(l) \\ \gamma = \sigma^2_1 / (\sigma_o \sigma_2); \qquad R_* = \sigma_1 / \sigma_2. \end{array} \tag{8}$$

D. Novikov and H. Jørgensen [6] have shown that the value of parameter γ determines the topology of the ΔT distribution on the sky as well as the rate of peak clusterisation which decreases with γ. According to [6] the mean length of clusters at threshold ν_t is

$$\langle k(\nu_t) \rangle = [1 - \alpha(\nu_t, \gamma)]^{-1}, \tag{9}$$

where $\alpha(\nu_t \gamma) = \widetilde{N}^+_{min}(\nu_t) / \widetilde{N}^+_{max}(\nu_t)$ and

$$\widetilde{N}^+_{max} = \frac{1}{4\pi} \frac{\sigma_2}{\sigma_1} \left\{ 1 - \Phi \left(\frac{\nu_t}{\sqrt{2(1-\gamma^2)}} \right) + \gamma e^{-\frac{\nu_t^2}{2}} \left[1 + \Phi \left(\frac{\gamma \nu_t}{\sqrt{2(1-\gamma^2)}} \right) \right] \right\}, \tag{10}$$

$$\widetilde{N}^+_{min} = \frac{1}{4\pi} \frac{\sigma_2}{\sigma_1} \left\{ 1 + \Phi \left(\frac{\nu_t}{\sqrt{2(1-\gamma^2)}} \right) - \gamma e^{-\frac{\nu_t^2}{2}} \left[1 - \Phi \left(\frac{\gamma \nu_t}{\sqrt{2(1-\gamma^2)}} \right) \right] \right\}, . \tag{11}$$

where $\Phi(x)$ is the error function [8]. In the next sections we discuss general properties of the parameter γ for different types of CMB spectra, $C(l)$, corresponding to different cosmological models (SCDM, ΛCDM, etc). Different strategies for the RATAN-600 observations will also be discussed.

3 Statistical properties of the ΔT-signal in the RATAN-600 scans.

In the framework of Cosmological Gene Project several modes (or strategies) of observations are possible (see [9]). Below we discuss only the SECTOR mode of radio sky observations where several $\frac{1}{4}$ parts of the RATAN-600 antenna ring with separated secondary mirrors may be used. Besides that, the beam-switching strategy in the SECTOR mode is very important for both AE and point sources filtration and detection of the primordial CMB signal.

Let us discuss one of the possible beam-switching regimes. In this case two radiometers are turned to one secondary mirror and measure the difference of the ΔT-signals between themselves:

$$\widetilde{\Delta T}_{II}(x) = \Delta T(x+d) - \Delta T(x), \tag{12}$$

where d is the angular distance between pointings of the radiometers. We find that

$$\widetilde{\Delta T}_{II}(x) \approx \frac{dT}{dx}|_{d=0}\, d \tag{13}$$

for the multipole numbers $ld \ll 1$. If d^{-1} corresponds to $l \sim 10^4 - 10^5$ then Eq.(13) is correct practically in all of the most important ranges of the observations for $l \leq 10^4 - 10^5$. Note, that due to the linear character of the Eq.(13), the distribution of $\widetilde{\Delta T}_{II}(x)$ is Gaussian. More over, the multipole spectrum of function $\Delta T_{II}(x)$ is connected with the multipole spectrum of the initial signal as

$$\widetilde{C}_{II}(l) = l^2 d^2 C(l). \tag{14}$$

Thus, as we can see, the analysis of the statistical properties of the first derivatives of the initial signal is practically equivalent to the analysis of the power spectrum $l^2C(l)$. In addition there are two main points which are very important for the future investigations. The first is the following. As we mentioned above, the high frequency noise, which is connected with the noise of a radiometer and other sources, are usually present in the observational atmospheric emission scans of RATAN-600 (see for example Fig.1a). These high frequency modulations can be extracted from the initial scan by smoothing over scales $\theta_S \simeq 5 - 15\text{arcsec} > d$ using a Gaussian filter for example:

$$\Delta T_{II}(x) = \frac{1}{\sqrt{2\pi}\theta_S} \int_{-\infty}^{\infty} \widetilde{\Delta T}_{II}(x') \exp\left[-\frac{(x-x')^2}{2{\theta_S}^2}\right] dx'. \tag{15}$$

The smoothing procedure in Eq.(15) leads to the following transformation of the power spectrum Eq.(14):

$$C_{II}(l) = l^2 d^2 C(l) e^{-l^2\theta_s^2}. \tag{16}$$

The second point is connected with general properties of the primordial spectrum $C(l)$ for the most popular cosmological models at high multipoles $l \geq 10^2$. As we mentioned in the introduction the spectrum has an exponential decrease due to damping at $l \succeq l_d \approx 10^3$: $C(l) \propto exp(-l^2 R_d^2)$ where $R_d \sim l_d^{-1}$.

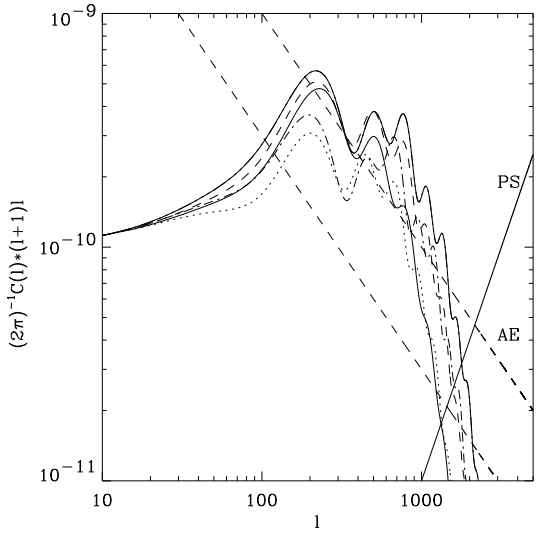

Figure 3: *Spectra of primordial CMB signal for different cosmological models (see Table 1). Straight dashed lines represent the spectrum of AE and the straight solid line represents spectrum for unresolved point sources (PS).*

Besides that, for the Harrison-Zeldovich initial power spectrum of adiabatic perturbations the typical trend of the multipole spectrum of CMB is $C(l) \propto l^{-2}$ at $l_d > l \gg 1$ with Sakharov's modulations. Moreover, we expect that for the AE fluctuations the spectrum of the noise is close to a power law spectrum as well. Similarly we get for the different types of the foreground, synchrotron emission, dust and free-free emission, $C(l) \sim l^{-3}$ [4] and $C(l) \sim l^0$ for the point sources.

Thus, for the future investigation we adopt the following form of the considered power spectrum $C_{II}(l)$:

$$
\begin{aligned}
&C_{II\ CMB}(l) \propto d^2 e^{-l^2(R_d^2+\theta_S^2)} l^q && for\ the\ primordial\ CMB\ signal \\
&C_{II\ PS}(l) \propto d^2 l^2 e^{-l^2\theta_S^2} && for\ PS\ noise \\
&C_{II\ atm}(l) \propto d^2 l^2 (1+l^2 a^2)^{-m} e^{-l^2\theta_S^2} && for\ AE\ noise
\end{aligned}
\tag{17}
$$

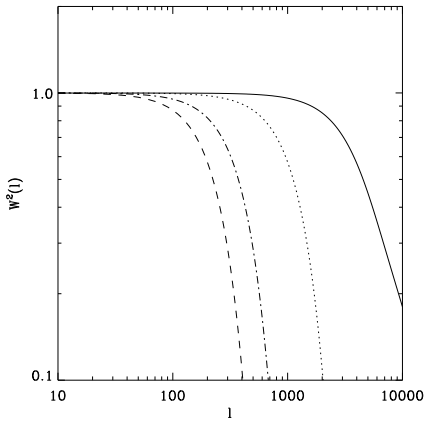

Figure 4: *Left panel represents the beam profile of the RATAN-600 antenna for the SECTOR mode at $\lambda = 1cm$. The right panel $W^2(l)$: solid line for RATAN-600 scans, dotted line for Planck HFI, dashed-dotted line for MAP and dashed line for PLANCK LFI.*

where $\Phi(l) = l^q e^{-l^2 R_d^2}$ describes Sakharov's modulations in the CMB spectra, a^{-1} is the typical scale in l-space for the power part of the AE spectrum; m and q are spectral indices.

The last point is connected with the shape of the antenna beam. For example, in the MAP and PLANCK satellite missions the Gaussian antenna beams correspond to $W^2(l) \propto \exp(-l^2\theta_A^2)$, $\theta_A \simeq 7.45 \times 10^{-3} \left(\frac{\theta_{FWHM}}{1^o}\right)$ [10], where $\theta_A = 2.23 \times 10^{-4}$ for the MAP project ($\theta_{FWHM} = 0.3^o$) and $\theta_A = 7.45 \times 10^{-4}$ for the HFI detector in PLANCK (($\theta_{FWHM} = 0.1^o$). The multipole character of the RATAN-600 antenna beam is more complicated than antenna beams of MAP and PLANCK. For $W(x, y) \geq 0.1$ we use the following expression [11]:

$$W(x,y) = \exp\left\{-(\gamma' y)^2 - \frac{1}{2}\ln[1 + (\alpha y)^2] - \frac{(\delta x)^2}{1 + (\alpha y)^2}\right\}, \tag{18}$$

where $\alpha = \frac{2\sqrt{3}}{FWHM(y)}$, $\delta = \frac{2\sqrt{\ln 2}}{FWHM(x)}$, $\gamma' = \frac{2\sqrt{\ln 2}}{FWHM(E)}$, and $FWHM$ is the standard definition of the "full-width-half-maximum" in the x and y directions and energy respectively. This description is applicable for the central part of the antenna beam and the parameters α, δ and γ' depend on the frequency of the observations. For example, at $\nu = 30$GHz the values of $FWHM$ are the following: $FWHM(x) = 5.1$ arcsec, $FWHM(y) = 37.7$ arcsec and $FWHM(E) = 717$ arcsec.

We determine the Fourier transformation of $W(x,y)$:

$$W_{ij} = (1 + k_\gamma^2 \mu^2)^{-1/2} \exp\left[-\frac{k_i^2}{4\delta^2} - \frac{k_j^2}{4(\gamma^2 + \frac{k_i^2 \alpha^2}{4\delta^2})} \right], \tag{19}$$

where $k_i = \frac{2\pi\ i}{L}$, $k_j = \frac{2\pi\ j}{L}$, $\mu = \alpha/2\gamma\delta$ and substitute W_{ij} from Eq.(19) in Eq.(5). After the transformation $l = \frac{2\pi}{L}\sqrt{i^2 + j^2}$ and integration over angle $\varphi = \arctan j/i$ we find the dependence $W^2(l)$ on l as follows

$$W^2(l) = \frac{2}{\pi} \int_0^1 \frac{dx\ \exp\{-P(x)\}}{\sqrt{1 - x^2}(1 + m^2(l)x^2)} \tag{20}$$

where $P(x) = d^2(l)x^2 + \frac{c^2(l)(1-x^2)}{1+m^2(l)x^2)}$, $d(l) = \frac{l}{\sqrt{2}\delta}$, $c(l) = \frac{l}{\sqrt{2}\gamma}$, $m(l) = l\ \mu$.

In Fig. 4 we have plotted $W^2(l)$ from Eq.(20). As one can show from this figure we can apply the following approximation for $W^2(l)$ practically up to $l \sim 10^4$:

$$W^2_{RATAN}(l) \simeq \left(1 + \frac{l^2}{l_0^2}\right)^{-1}, \tag{21}$$

where $l_0 = 4.5 \times 10^3$.

Taking into account notations mentioned above (see Eq.(7) and Eq.(8)), we determine spectral parameters σ_p^2 for $C_{II}(l)$ from Eq.(3) and definition Eq.(9):

$$\sigma^2_{p,CMB} = \frac{\pi\ d^2\ A}{2(l_0^2)^{p+1+q/2}} \Gamma\left(p + 1 + \frac{q}{2}\right), \tag{22}$$

$$\sigma^2_{p,PS} = \frac{\pi\ d^2\ B}{2\theta_S^{2(p+2)}} \Gamma\left(p + 2\right), \tag{23}$$

$$\sigma^2_{p,AE} = \frac{\pi\ d^2\ C}{2a^2\theta_S^{2p+1}} \Gamma\left(\frac{1}{2} + p\right), \tag{24}$$

where $\Gamma(x)$ is the *gamma*-function. For the AE spectrum in Eq.(3) we took $m = 3/2$, and A, B, C are amplitudes of the CMB, PS and AE power spectra.

Let us discuss some exact values of the parameter γ for the CMB, PS and AE signals. For σ_p^2 from Eq.(22)-Eq.(24) all γ parameters (Eq.(8)) have extremely simple expressions:

$$\gamma_{CMB} = \sqrt{\frac{q+2}{q+4}}; \qquad \gamma_{PS} = \sqrt{\frac{2}{3}} = 0.82; \qquad \gamma_{AE} = \frac{1}{\sqrt{3}} = 0.58. \tag{25}$$

For realistic values of $q \simeq 0 - 2$ the corresponding values of γ are $\gamma_{CMB} = 0.77$ at $q = 1$ and $\gamma_{CMB} = \sqrt{\frac{2}{3}} = 0.82$ at $q = 2$. As one can see from Eq.(25) we have for the AE

noise, $\gamma_{AE} \simeq 0.58$ which is less than γ_{CMB} and γ_{PS}. Therefore the rate of AE noise clusterisation is larger than the rate of the CMB and PS clusterisation referring to [6].

We compared our analytical predicted parameters γ with the data of numerical simulations of this parameter from real theoretical CMB spectrum $C_{II\ CMB}(l)$ using the CMBFAST code [""""]. We used the results only of this numerical simulation and $W(l)$ for the RATAN-600 antenna (see Fig.4b). The results are presented in Table 1. As one can see from this table, the values of the parameter γ for all investigated SCDM models are close to the value of $\overline{\gamma}_{CMB} \simeq 0.79$ and differing less than 4%. This means that the value of the parameter $\overline{\gamma}_{CMB}$ corresponds to $q \simeq 1-2$. For the ΛCDM model (see Table 1) a more preferable value of parameter q is $q \simeq 0$.

Thus, as the result of our analytical investigation of the CMB, AE and PS spectra we have the following important conclusions. For different CMB power spectra the values of parameter γ_{CMB} and the rate of clusterisation practically coincide. The AE noises due to more sloping character of initial spectrum is clusterized more strongly than the primordial CMB signal and PS noise.

4 Turning points of the peak clusterisation.

As we have shown in the previous section, the spectral parameters σ_p^2 for different types of signals characterize the topology of Gaussian maps corresponding to the different types of noise. In practice we have a combination of the primordial CMB signal, AE noise, foreground and PS. Therefore the topology of the map and the structure of a single scan are more complicated than topology of "pure" CMB, AE, PS and other signals. In this case the rate of peak clusterisation at different threshold levels ν_t is described in terms of the parameter γ_{tot} if we suppose that all types of noise are Gaussian. Thus for mixed CMB+AE+PS+foreground sources the topology of a map can be described in terms of γ_{tot}:

$$\gamma_{tot} = \sum_{i=1}^{N}(\sigma_1^2(i))\left\{\sum_{i=1}^{N}\sigma_0^2(i)\sum_{i=1}^{N}\sigma_2^2(i)\right\}^{-1/2}, \tag{26}$$

where $\sigma_p^2(i)$ are given by Eq.(22)-(24), i is a number of the type of noise and CMB signal, N is a total number of different types of noise and the CMB signal [4].
Let us introduce new functions:

$$X = \frac{\sigma_0^2(PS)}{\sigma_0^2(CMB)}; \qquad Y = \frac{\sigma_0^2(AE)}{\sigma_0^2(CMB)}. \tag{27}$$

[4]For the most important types of foreground such as synchrotron emission, dust and free-free emission we have a power spectrum $C(l) \sim l^{-3}$. We denote a sum of this type of noises as σ_{AE}^2, if the variance of the AE signal dominates. It is natural that methods of filtration for different types of noise can be different.

Using Eq.(26), (27) and (22)-(24) we have the following expression for the parameter

$$\gamma_{tot}(X,Y,\xi) = \frac{1}{\sqrt{2}} \frac{\left[1+\xi(2X+\frac{1}{2}Y)\right]}{\left[(1+X+Y)(1+\xi(3X+3/8Y)\right]^{1/2}}, \tag{28}$$

where $\xi = 1 + \frac{R_d^2}{\theta_S^2}$ and we adopt $q = 0$ for CMB signal.

Note that the parameter ξ describes the dependency of the function γ_{tot} of the angular resolution of the antenna beam and can be $\approx$1 if $\theta_S \gg R_d$ (for example for MAP project) and $\xi \gg 1$ if $\theta_S \ll R_d$ (for the RATAN-600 antenna beam). Thus, the angular sensitivity of the antenna plays a critical role in our cluster analysis technique.

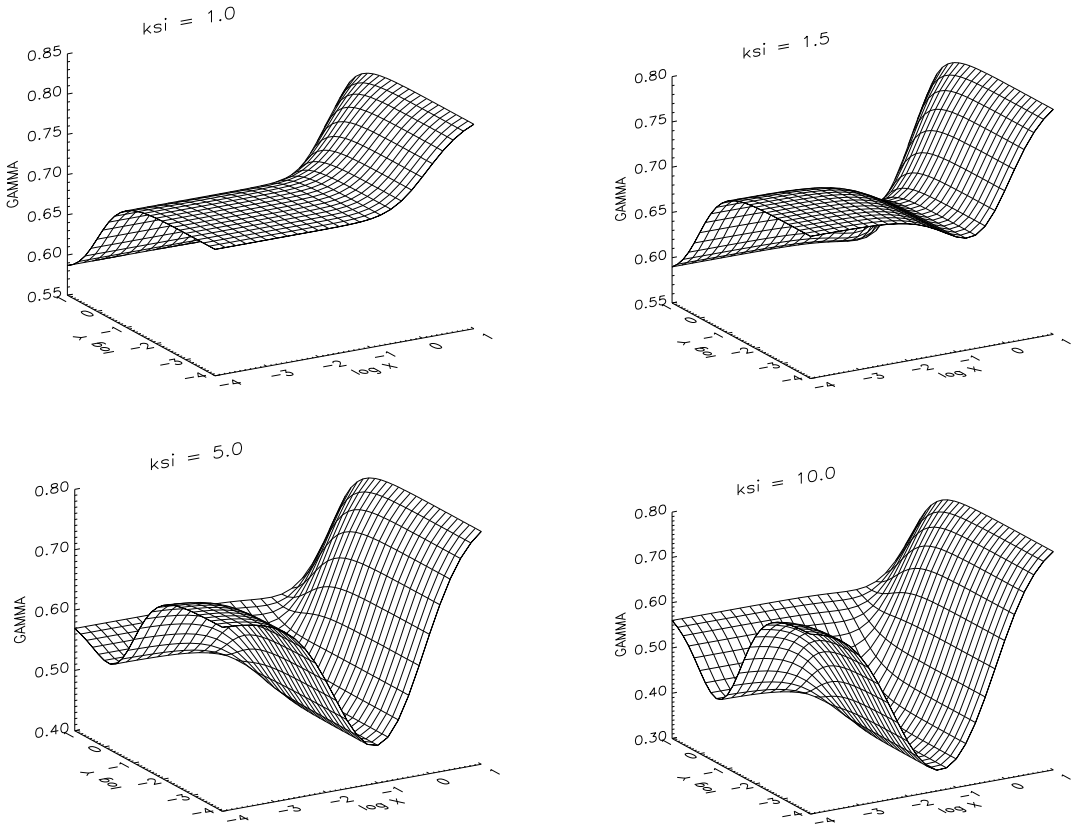

Figure 5: $\gamma(X,Y,\xi)$-*surfaces. Top left for* $\xi = 1$*, top right for* $\xi = 1.5$*, bottom left for for* $\xi = 5$ *and bottom right for* $\xi = 10$*.*

In Fig. 5 we have plotted the function $\gamma_{tot}(X,Y,\xi)$ for different values of $\xi = 1, 1.5, 5, 10$. As seen from this figure, the shape of $\gamma_{tot}(X,Y,\xi)$ surfaces at different values of parameter ξ is very complicated. In Fig. 6 we represent two types of cross

sections of $\gamma_{tot}(X, Y, \xi)$ surfaces. Panel a-c shows $\gamma_{tot}(X, Y_n, \xi)$ as function of X for $Y_n = 10^{-3} - 1$ and $\xi = 1, 5, 10$. Panel d-f shows $\gamma_{tot}(X_n, Y, \xi)$ as function of Y for $X_n = 10^{-3} - 1$ and $\xi = 1, 5, 10$.

Thus the surface $\gamma_{tot}(X, Y, \xi)$ describes the dependence of the main parameter of peak clusterisation based on different procedures of AE and foreground filtration. For the AE noise filtration one of the most important methods is the averaging of observational scans over ensembles. Due to the averaging procedure the variance of AE noise decreases in time as t^{-1}. Increasing the observing time leads to a decrease of the parameter Y (keeping $X = const$). Using Fig. 5 we can estimate the trajectory $X(Y)$ which corresponds to any filtration procedure.

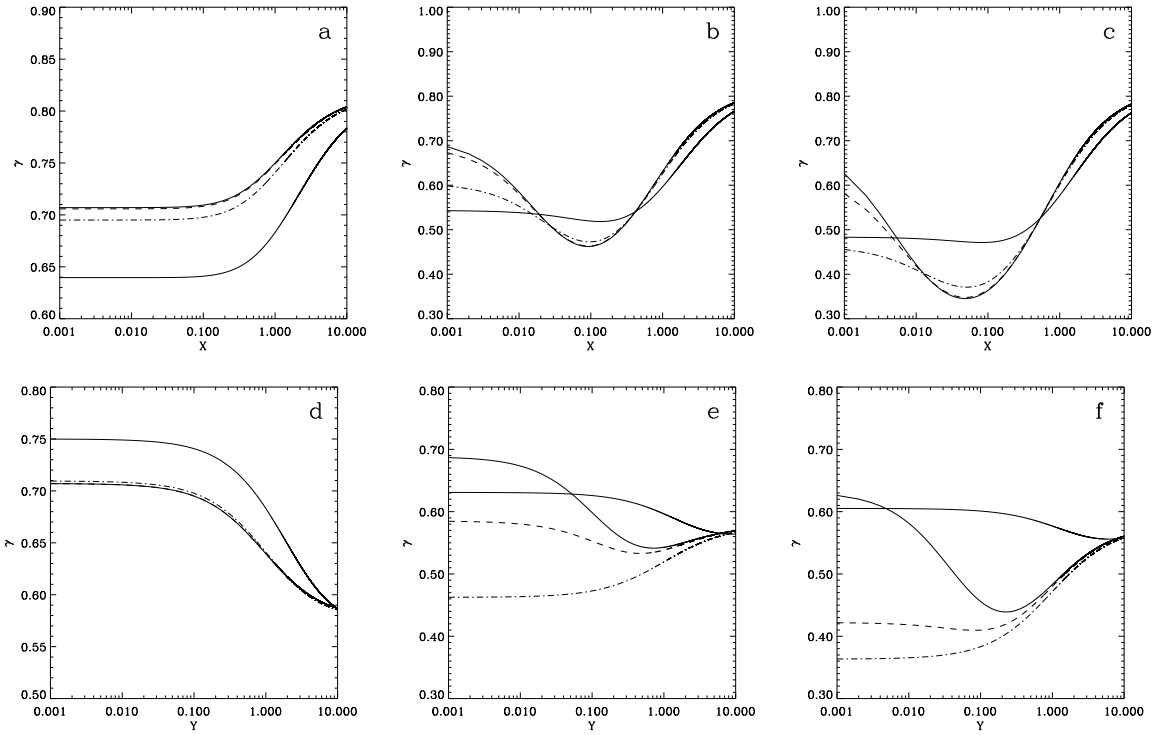

Figure 6: *a)* $\gamma(X, Y_n, \xi = 1)$ *at* $Y_n = 0.001$ *(thin solid line),* $Y_n = 0.01$ *(dashed line),* $Y_n = 0.1$ *(dashed-dotted line) and* $Y_n = 1$ *(thick solid line). b) and c) are the same as in a) but for* $\xi = 5$ *and* $\xi = 10$ *respectively. d)* $\gamma(X_n, Y, \xi = 1)$ *for* X_n*=0.001 (thin solid line),*X_n*= 0.01 (dashed line),* X_n*=0.1 (dashed-dotted line); and* X_n*=1, (thick solid line); e) and f) are the same as in d) but for* $\xi = 5$ *and* $\xi = 10$ *respectively.*

Let us assume that the variance of AE signal is greater than those of the PS and CMB signals. In this case a typical value of parameter $\gamma(X, Y, \theta_S)$ is $\gamma \simeq \frac{1}{\sqrt{3}}$. If the angular resolution of the antenna beam corresponds to $\xi \simeq 1$ then after averaging

Table 1: Numerical values of γ-parameter for different cosmological models.

SCDM						ΛCDM
$H_0 = 50$			$H_0 = 75$			$H_0 = 75$
Ω_b			Ω_b			Ω_b
0.0125	0.025	0.05	0.0125	0.025	0.05	0.0125
γ			γ			γ
0.82	0.77	0.78	0.82	0.76	0.79	0.72

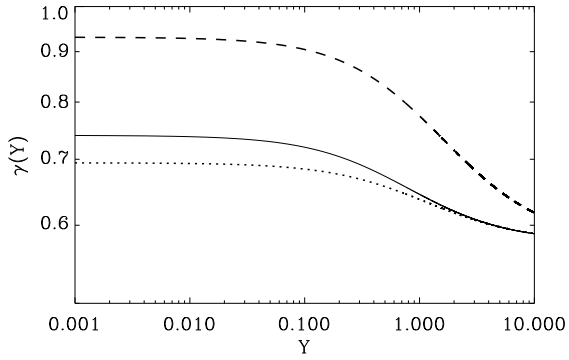

Figure 7: *Parameter $\gamma_{tot}(Y)$ for $l_S = 10^2$ (dashed line), $l_S = 5 \times 10^2$ (solid line), and $l_S = 10^3$ (dotted line).*

the signal the parameter $\gamma(X = 0, Y, \theta_S)$ monotonically transforms from $\gamma \simeq \frac{1}{\sqrt{3}}$ to $\gamma \simeq \frac{1}{\sqrt{2}}$ (see Fig.6). This means that the rate of the maxima clusterisation decreases monotonically. However, we would like to point out that for $\xi > 1$, for example $\xi \simeq 10$, which is close to the RATAN-600 antenna characteristics, the situation changes drastically. In this case during the averaging procedure the value of the γ parameter decreases with time while the rate of clusterisation increases. This process continues up to the moment when γ reaches its minimum at some moment of time t_{cr}. At $t > t_{cr}$ the value of γ goes up and the rate of clusterisation monotonically decreases. We name the point $t = t_{cr}$ when γ reaches its minimum, as "the turning point" of the maximum clusterisation.

As one can see from Fig. 6 the existence of such points is natural both for AE+CMB signals and for all types of foregrounds. For a specific value of ξ (for a specific antenna) the turning points form a line $X = X(Y)$ in the plane(X, Y). This non-trivial behavior of the parameter γ gives new possibilities for separating the primordial CMB signal from noise.

Finally we consider in more detail the dependence of γ on Y when $\theta_S \leq R_d$ which corresponds to the range of the spectrum with $l \leq l_d \approx 10^3$. For this range of l we can neglect the damping decrease of the CMB spectrum. At $10^2 < l < 10^3$ CMB spectrum has a few maxima and we will use the exact numerical description of the spectrum of CMB. For simplicity we will consider a case where PS noise is not important for this range of l and we will consider CMB+AE signal only. We have plotted the corresponding dependence $\gamma_{tot}(Y, \theta_S)$ in Fig. 7 for a SCDM power spectrum and AE noise and for $l_S = 10^2$, $l_S = 5 \times 10^2$ and $l_S = 10^3$, where $l_S \sim \theta_S^{-1}$.

As one can see from this figure the shape of $\gamma_{tot}(Y, \theta_S)$ is monotonic and increases from $\gamma_{tot} \simeq \frac{1}{\sqrt{3}}$ up to $\gamma_{tot} \simeq 0.92$ (for $\theta_S = 10^{-2}$) if Y decreases. This means that in the range $10^2 < l_S < 10^3$ we have practically the same behavior of γ parameter as in Figure 6d.

5 Conclusions

The main goal of this paper was to develop the cluster analysis of the one-dimensional random fields in the application to the RATAN-600 observational scans for measurements of the CMB anisotropy. We analyzed the properties of the peak clusterisation in the RATAN-600 scans and demonstrated how the high angular resolution of the antenna of RATAN-600 can be used to reveal noise related to atmospheric emission and unresolved point sources in the observational data.

We believe that the cluster analysis method will find its place in the future data reduction of ground based experiments together with other published methods of AE filtration.

Acknowledgments

P.N. is grateful to the staff of TAC, and NORDITA for providing excellent working conditions during his visit to these institutions. This investigation was supported in part by a grant ISF MEZ 300, by a grant INTAS 97-1192, by the Danish Natural Science Research Council through grant No 9701841 and by Danmarks Grundforskningsfond through its support for the establishment of the Theoretical Astrophysics Center.

References

1. B. Melchiorri, M. de Petris, G.D'andreta, G. Guarini, F. Melchiorri and M. Signore; *Astrophys. J.*, **471**, 52, (1996).
2. O. Lay, N. Halverson, Astroph/9905369 (1999).
3. W., Hu, http:/www/sns.ias.edu.
4. M. Tegmark, D. Eisenstein, W.Hu, A. de Oliviera-Costa; Astroph/9905257 (1999).
5. P. Naselsky, and D. Novikov, *Astrophys. J.*, **444**, L1, (1995).
6. D. Novikov and H. Jørgensen, *Astrophys. J.*, **471**, 521, (1996).
7. Bond., Y.R., and G.Efstathiou, *Mon. Not. Roy. Astro. Soc*, **226**, 655, (1987).

8. I.S. Gradstein, Ryzhik, I.M. " *Tables of Integrals, Series and Products* Ed. by Alan Jeffrey Academic Press, (1980).
9. P. Naselsky, I. Novikov, Yu Parijskij, P. Tcibulev; Internationa Journal of Moden Physics, **8**, n5, (1999)
10. G. Jungman, M. Kamionkowski, A. Kosowsky, D. Spergel; *Phys. Rev. D* **54**, 1332, (1996).
11. A.V. Chepurnov; PhD thesis (1997).